

# The absorption spectrum of the QSO PKS 2126–158 ( $z_{\text{em}} = 3.27$ ) at high resolution <sup>\*</sup>

V. D’Odorico<sup>1</sup>, S. Cristiani<sup>2</sup>, S. D’Odorico<sup>3</sup>, A. Fontana<sup>4</sup>, and E. Giallongo<sup>4</sup>

<sup>1</sup> International School for Advanced Studies, SISSA, via Beirut 2-4, I-34014 Trieste, Italy

<sup>2</sup> Dipartimento di Astronomia dell’Università di Padova, Vicolo dell’Osservatorio 5,  
I-35122 Padova, Italy

<sup>3</sup> European Southern Observatory, Karl Schwarzschild Strasse 2, D-85748 Garching, Germany

<sup>4</sup> Osservatorio Astronomico di Roma, via dell’Osservatorio, I-00040 Monteporzio, Italy

Received ...; accepted ...

**Abstract.** Spectra of the  $z_{\text{em}} = 3.268$  quasar PKS 2126–158 have been obtained in the range  $\lambda\lambda 4300 - 6620 \text{ \AA}$  with a resolution  $R \simeq 27000$  and an average signal-to-noise ratio  $s/n \simeq 25$  per resolution element. The list of the identified absorption lines is given together with their fitted column densities and Doppler widths. The modal value of the Doppler parameter distribution for the Ly $\alpha$  lines is  $\simeq 25 \text{ km s}^{-1}$ . The column density distribution can be described by a power-law  $dn/dN \propto N^{-\beta}$  with  $\beta \simeq 1.5$ .

12 metal systems have been identified, two of which were previously unknown. In order to make the column densities of the intervening systems compatible with realistic assumptions about the cloud sizes and the silicon to carbon overabundance, it is necessary to assume a jump beyond the He II edge in the spectrum of the UV ionizing background at  $z \sim 3$  a factor 10 larger than the standard predictions for the integrated quasar contribution.

An enlarged sample of C IV absorptions (71 doublets) has been used to analyze the statistical properties of this class of absorbers strictly related to galaxies. The column density distribution is well described by a single power-law, with  $\beta = 1.64$  and the Doppler parameter distribution shows a modal value  $b_{\text{CIV}} \simeq 14 \text{ km s}^{-1}$ . The two point correlation function has been computed in the velocity space for the individual components of C IV features. A significant signal is obtained for scales smaller than  $200 - 300 \text{ km s}^{-1}$ ,  $\xi(30 < \Delta v < 90 \text{ km s}^{-1}) = 32.71 \pm 2.89$ . A trend of decreasing clustering amplitude with decreasing column density is apparent, analogously to what has been observed for Ly $\alpha$  lines.

**Key words:** quasars: absorption lines – quasars: individual: PKS 2126–158

*Send offprint requests to:* Stefano Cristiani

<sup>\*</sup> Based on observations collected at the European Southern Observatory, La Silla, Chile (ESO No. 2-013-49K).

## 1. Introduction

The study of quasars at high redshift has gained, in the last years, a remarkable position in cosmology because of its important contribution to the knowledge of the formation and evolution of cosmological structures. Besides the study of the quasar population itself, the analysis of the quasar absorption spectra allows us to probe the intervening matter up to the redshift of the emitting object.

Thanks to the improvement in astronomical instrumentation, a considerable amount of high resolution data has become available in recent years, greatly increasing the knowledge of the nature and evolution of the absorbers.

The absorption spectra of QSOs at high redshifts are characterized by a “forest” of lines shortward of the Ly $\alpha$  emission, first noted by Lynds (1971), who correctly interpreted them as Ly $\alpha$  due to absorbers distributed along the line of sight.

The large range in column densities of these lines suggests the presence of very different intervening structures, from fluctuations of the diffuse intergalactic medium to the interstellar medium in protogalactic disks.

Profile fitting techniques (e.g. Fontana & Ballester 1995; Hu et al. 1995) provide the few parameters (redshift  $z$ , Doppler width  $b$  and column density  $N$ ) constituting the basis for the interpretation of the physical properties of the absorbers. The reliability of such parameters depends strongly upon the resolution and the signal to noise ratio of the spectral data. Controversies arisen in the past may be traced back to the difficulty of the observational problem, at the limit of the present technology (Pettini et al. 1990; Carswell et al. 1991; Rauch et al. 1993).

Remarkable results have been recently obtained in the study of the clustering properties of Ly $\alpha$  clouds. The ab-

sence of clustering for velocity separations between 300 and 30000 km s<sup>-1</sup> has been assessed (Sargent et al. 1980,1982; Bechtold et al. 1987; Webb & Barcons 1991). On the other hand, the presence of a significant non-zero correlation function has been observed for Ly $\alpha$  lines with  $\Delta v < 300$  km s<sup>-1</sup> and  $\log N_{\text{HI}} \gtrsim 13.8$  (Chernomordik 1995; Cristiani et al. 1995; Meiksin & Bouchet 1995, Hu et al. 1995; Fernández-Soto et al. 1996). The correlation function for the present sample of Ly $\alpha$  lines is discussed in Cristiani et al. (1997).

Lanzetta et al. (1995) inferred from observational results that, at  $z \leq 1$ , at least 32 % (but it could be as high as 60 %) of the Ly $\alpha$  absorption systems arise in luminous galaxies. This conclusion is at variance with the longstanding belief that Ly $\alpha$ -forest absorption systems arise in intergalactic clouds. Moreover, recent spectra at very high resolution have revealed the presence of C IV absorptions associated with Ly $\alpha$  lines with  $\log N_{\text{HI}} \gtrsim 14$  (Cowie et al. 1995; Tytler et al. 1995; Womble et al. 1996; Songaila & Cowie 1996). The derived abundances seem to be similar to the ones derived for the heavy elements absorptions originated in galactic halos, suggesting continuity in their physical properties.

The clustering of C IV absorption systems has been investigated in the past using large samples observed at low resolution - FWHM  $> 1 \text{ \AA}$  - (33 QSOs in Young et al. 1982; 55 QSOs in Sargent et al. 1988 ). From these data it has been possible to assess that C IV systems do cluster on scales  $\Delta v \lesssim 600$  km s<sup>-1</sup>, but, due to the limited spectral resolution, the characteristic clustering scale and the clustering properties at smaller velocity separations have not been established.

Petitjean and Bergeron (1994) analyzed a sample of 10 QSOs with a higher spectral resolution. They obtained as best fit of the two point correlation function in the range 30 – 1000 km s<sup>-1</sup> a sum of two Gaussian components with dispersions of 109 and 525 km s<sup>-1</sup>, similar to the distribution observed for Mg II systems (Petitjean & Bergeron 1990). This result further confirms that metal systems as identified by C IV absorptions features arise in galactic halos.

More recent works by Womble et al. (1996) and Songaila and Cowie (1996) analyzed clustering of lower column density samples detecting a lower signal on the same scales studied by Petitjean and Bergeron (1994). This trend with column density is consistent with what is observed for Ly $\alpha$  lines (see Cristiani et al. 1997).

In the present paper we address these issues on the basis of the absorption spectrum of the quasar PKS 2126–158 ( $z_{\text{em}} = 3.268$ ). This object is one of the brightest quasars known ( $m_V \simeq 17.1$ ) and for this reason its spectrum has been studied in many previous works (Jauncey et al. 1978; Young et al. 1979; Sargent & Boksenberg 1983; Meyer & York 1987; Sargent et al. 1988; Sargent et al. 1989; Sargent et al. 1990; Giallongo et al. 1993 hereafter GCFT). Here

we present new data, providing improved quality spectra in terms of  $s/n$  ratio, resolution and wavelength range.

The paper is organized as follows. In Sec. 2 we describe the observations and the data reduction, in Sec. 3 the method of analysis. Section 4 discusses the statistical properties of the Ly $\alpha$  sample. The description of the metal-line systems is given in Sec. 5. Section 6 analyses some statistical properties of the C IV absorption systems. In Sec. 7 the two point correlation function is computed for the C IV lines and the correlation between clustering and column density is investigated. The conclusions of the paper are in Sec. 8.

## 2. Data acquisition and reduction

In August 1991 and August 1994, 8 echelle observations of the quasar PKS 2126–158 were obtained at ESO (La Silla), with the NTT telescope and the EMMI instrument (see D’Odorico 1990). The ESO echelle #10 was used in the red arm of the instrument in combination with a grism cross-disperser. The seeing during the observations was typically between 0.8 and 1.3 arcsec.

The absolute flux calibration was carried out by observing the standard star EG274 (Stone & Baldwin 1983).

The data have been reduced in the context of the ECHELLE software package available in the 94NOV edition of MIDAS, the ESO data reduction system. Some improvements have been introduced with respect to the standard procedure. In particular, the spectra obtained from different observations are summed up without a previous rebinning but maintaining the original pixel sampling. For the wavelength calibration Thorium lamp spectra have been used. Wavelengths have then been corrected to vacuum heliocentric.

The weighted mean of the spectra is equivalent to  $\sim 16$  hours of integration time and it presents a resolution  $R \simeq 27000$ . The  $s/n$  ratio per resolution element at the continuum level is doubled compared with the previous spectrum by GCFT: it ranges from  $s/n \simeq 6$  to 44 in the interval 4380 – 5190 Å, while beyond the Ly $\alpha$  emission it has a roughly constant value of  $s/n \simeq 30$ .

In addition to these data, 8 long slit observations of the spectrum of PKS 2126–158 were obtained with an holographic grating (ESO #11) at the blue arm of the EMMI instrument. The reduction has been carried out with the LONG SLIT package of MIDAS, using an optimal extraction option. The resolution of these data is  $R \sim 8500$ .

The resulting spectrum has been used to check the reliability of the Ly $\alpha$  identification process by verifying the presence of the higher order Lyman series lines.

The journal of the observations is given in Tab. 1.

**Fig. 1.** Spectrum of PKS 2126–158 in the wavelength range  $\lambda\lambda 4300 - 6620$  covered by the new observations showing fits to identified lines overlaid upon the normalized spectrum. The spectral interval  $\lambda\lambda 6620 - 7000$  and the corresponding absorption lines are shown in GCFT. The dashed line represents the noise per resolution element. Upper vertical ticks correspond to Ly $\alpha$  lines, lower ticks correspond to metal lines.

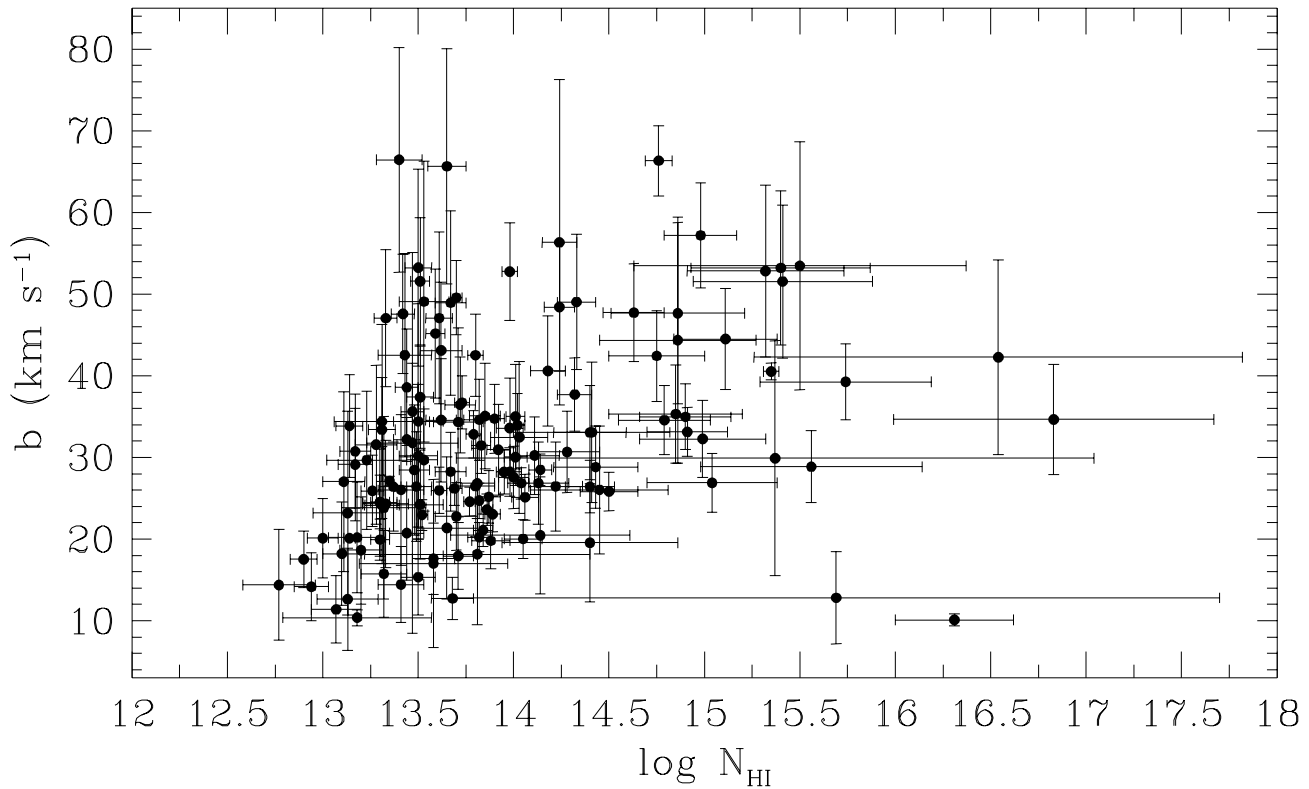


**Fig. 2.** Plot of the Doppler parameter  $b$  vs. the logarithmic column density  $\log N_{\text{HI}}$  for the Ly $\alpha$  lines listed in Tab. 2.

### 3. The detection and measurement of absorption lines

The determination of the continuum in the QSO spectrum is a critical step because it affects the measurement of the absorption line parameters. While the continuum redward of Ly $\alpha$  emission can be drawn without difficulty, the high line density in the Lyman forest complicates the operation (Young et al. 1979, Carswell et al. 1982). In the present work, the task has been fulfilled with the help of a procedure, allowing to select automatically and in a reproducible way the regions of the spectrum free of strong absorption lines or artificial peaks (e.g. due to cosmic rays), i.e. where the RMS fluctuation about the mean becomes consistent with noise statistics. The continuum level has been estimated by spline-fitting these regions with quadratic polynomials. The normalized spectrum is shown in Fig. 1.

The detection and measurement of absorption lines in the spectrum have been carried out as in GCFT and we refer to this paper for details of the procedure. In particular, the lines have been fitted with Voigt profiles convolved with the instrumental spread function, making use of a minimization method of  $\chi^2$ . This step has been performed within the MIDAS package with the programme FITLYMAN (Fontana & Ballester 1995). The values of redshift  $z$ , Doppler parameter  $b = \sqrt{2}\sigma$  (where  $\sigma$  is the velocity dispersion) and column density  $N$  have been determined for isolated lines and individual components of blends.

The number of components of each absorption feature is assumed to be the minimum required to give a reduced  $\chi^2 < 1$  (corresponding to a confidence level  $P \gtrsim 50\%$ ).

The identification of the metal systems is described in Sect. 5.

All the lines shortward of the Ly $\alpha$  emission not identified as due to metals have been fitted as Ly $\alpha$  and Ly $\beta$ . For

**Table 1.** Journal of the observations.

date (yy mm dd)	exposure (s)	slit width	range (Å)	CCD
91 08 06	7200	1".5	4539-7055	FORD 2k
91 08 06	7200	1".5	4539-7055	FORD 2k
91 08 07	9130	1".5	4539-7055	FORD 2k
94 08 13	5380	1".0	4056-6635	TK 2k #36
94 08 13	7200	1".0	4056-6635	TK 2k #36
94 08 13	7200	1".0	4056-6635	TK 2k #36
94 08 15	7200	1".2	4279-6644	TK 2k #36
94 08 15	6645	1".2	4279-6644	TK 2k #36
94 08 14	2700	1".2	3822-3980	TK 1k #31
94 08 14	2700	1".0	3822-3980	TK 1k #31
94 08 14	2700	1".0	3686-3846	TK 1k #31
94 08 14	2700	1".0	3686-3846	TK 1k #31
94 08 15	3600		3825-3983	TK 1k #31
94 08 15	3600		3825-3983	TK 1k #31
94 08 15	3600		3687-3848	TK 1k #31
94 08 15	3000		3687-3848	TK 1k #31

a further control, we used the blue, lower-resolution spectra to search for Ly $\beta$ , Ly $\gamma$  and Ly $\delta$  lines in correspondence to the stronger Ly $\alpha$  lines ( $\log N_{\text{HI}} \geq 14$ ). In few cases, we could ascertain that the absorption was not Ly $\alpha$ . Such lines are listed as unidentified in Tab. 2 and they probably belong to metal systems still to be recognized.

#### 4. Lyman alpha statistics

A statistically well-defined sample of Ly $\alpha$  lines in the region between the Ly $\beta$  and Ly $\alpha$  emissions ( $\lambda\lambda 4380 - 5191$ ) can be obtained from Tab. 2. The Ly $\alpha$  lines affected by the proximity effect ( $8h_{100}^{-1}$  Mpc from the QSO; see Bajtlik et al. 1988; Lu et al. 1991) and those associated with metal systems (indicated as M Ly $\alpha$ ) are excluded from the sample.

The distribution of lines in the  $b - \log N$  plane is shown in Fig. 2. The lack of lines at the top left corner can be ascribed to an observational bias: as already shown by GCFT, the selection criterion tends to miss lines with low column density and large Doppler width.

The dataset can be considered virtually complete (for typical  $b$  values) for  $\log N_{\text{HI}} \gtrsim 13.3$ .

A considerable fraction of the lines with  $\log N_{\text{HI}} \gtrsim 14.5$  belongs to complex saturated systems. As a consequence, the deblending choices and therefore the fitting parameters may be not always unique. A considerable improvement can be obtained when the simultaneous fit of the saturated Ly $\alpha$  and the corresponding Ly $\beta$  line is possible. Unfortunately, due to the high density of Ly $\alpha$  lines at these redshifts, Ly $\beta$  absorptions with an uncontaminated profile are rare and the uncertainty for most of the lines in the right region of the diagram 2 cannot be removed.

Simulations carried out by Fontana and Ballester (1995) show that, for isolated, unsaturated lines at  $s/n \gtrsim 8$ , the parameters given by the fitting procedure are quite close to the “true” value, with a small and symmetric scatter around it. At column densities larger than  $10^{14.5}$  cm $^{-2}$  the Ly $\alpha$  lines are saturated and  $b$  and  $N$  correlate strongly, increasing the uncertainties.

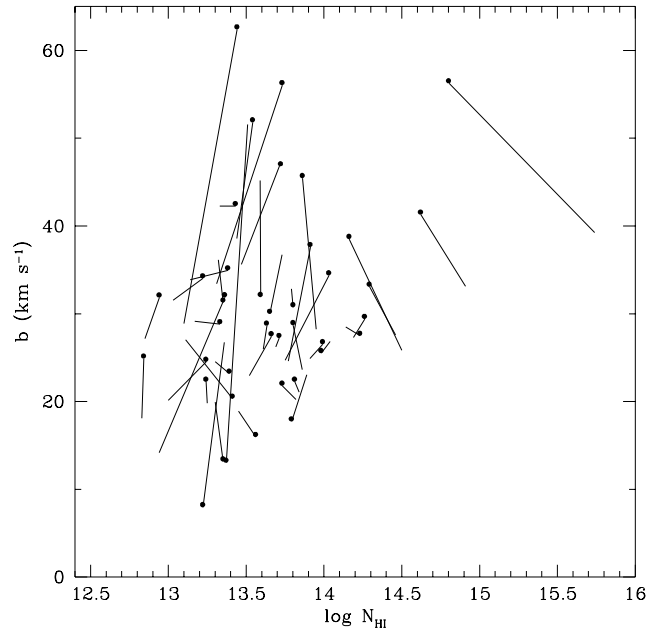


**Fig. 3.** Migration diagram illustrating the effect of improving the  $s/n$  ratio on the determination of the absorption lines parameters. The points correspond to the GCFT determination.

By comparing our list of lines with that published by GCFT, we have verified on real data how the  $b - \log N$  diagram changes when the average  $s/n$  ratio is almost doubled, checking the trends expected on the basis of simulations.

To carry out a meaningful comparison, we have considered only the isolated Ly $\alpha$  lines in common between the two line lists, at wavelengths  $\lambda > 4750$  Å. In this range the  $s/n$  per resolution element is  $\gtrsim 8$ . The lines are listed in Tab. 3.

Figure 3 shows the individual trajectory of each absorption line in the plane  $b - \log N$ . GCFT parameter values are indicated by the solid black circles and our values correspond to the end of the adjoining line.

Saturated lines tend to move keeping approximately constant the equivalent width value, as observed in the simulations (Fontana & Ballester 1995). Often they correspond to complex features. If the improved  $s/n$  is not sufficient for a proper deblending, but the better defini-





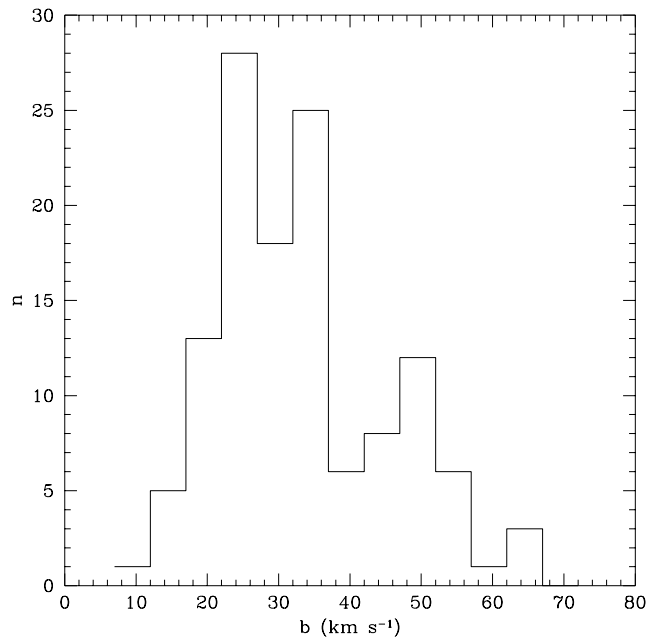


**Table 3.** Isolated lines in common between this sample and that of GCFT.

#	Present work			GCFT sample		
	$\lambda_{\text{vac}}(\text{\AA})$	$\log N$	$b$	$\lambda_{\text{vac}}(\text{\AA})$	$\log N$	$b$
1	4783.51	13.47	35.62	4783.72	13.72	47.09
2	4808.53	14.91	33.13	4808.30	14.62	41.59
3	4818.06	15.74	39.26	4817.86	14.80	56.55
4	4829.85	14.50	25.84	4829.67	14.16	38.82
5	4841.99	13.73	36.72	4841.83	13.65	30.28
6	4843.75	13.82	20.23	4843.61	13.73	22.10
7	4864.48	13.31	33.41	4864.25	13.73	56.34
8	4868.72	13.95	28.22	4868.49	13.86	45.75
9	4881.81	13.11	27.04	4881.50	13.41	20.62
10	4883.56	13.59	45.18	4883.55	13.59	32.21
11	4885.29	13.17	29.13	4885.17	13.33	29.11
12	4892.98	13.79	32.84	4892.90	13.80	31.03
13	4896.47	14.14	28.48	4896.26	14.23	27.78
14	4926.34	13.51	51.57	4926.28	13.37	13.32
15	4929.33	13.69	26.21	4929.10	13.71	27.53
16	4930.68	13.61	25.96	4930.46	13.63	28.94
17	4950.41	13.44	38.58	4950.44	13.54	52.10
18	4958.86	13.77	24.59	4958.70	13.91	37.90
19	4989.55	13.30	24.55	4989.60	13.39	23.47
20	4994.34	13.84	21.08	4994.23	13.81	22.55
21	5001.80	13.00	20.12	5001.91	13.24	24.82
22	5003.64	12.94	14.17	5003.67	13.36	32.17
23	5010.85	13.14	33.86	5010.40	13.38	35.23
24	5020.79	13.30	19.94	5020.84	13.35	13.48
25	5041.69	14.04	26.85	5041.48	13.98	25.82
26	5050.05	13.89	23.05	5049.84	13.79	18.03
27	5051.05	13.86	23.62	5050.83	13.80	29.00
28	5055.37	13.75	24.71	5055.22	14.03	34.67
29	5062.65	13.52	22.96	5062.51	13.66	27.73
30	5065.30	14.46	27.59	5065.08	14.29	33.37
31	5073.73	13.36	26.76	5073.34	13.22	8.26
32	5099.63	13.10	28.88	5099.25	13.44	62.69
33	5118.56	13.91	24.91	5118.41	13.99	26.83
34	5119.60	13.45	18.90	5119.37	13.56	16.25
35	5143.81	14.19	27.28	5143.64	14.26	29.70
36	5150.82	13.32	36.15	5150.61	13.35	31.57
37	5155.51	12.83	18.10	5155.42	12.84	25.19
38	5162.33	12.85	27.16	5162.03	12.94	32.15
39	5167.94	13.03	31.53	5167.80	13.22	34.33
40	5170.47	13.25	19.81	5170.31	13.24	22.54
41	5185.15	13.33	42.25	5184.94	13.43	42.56

tion of the wings forces a fit with a lower  $b$  parameter, then they move toward higher column densities.

Lines with low column density in regions with low  $s/n$  ratio have poorly defined profiles and are very sensitive to the continuum level. The  $s/n$  increase, together with a choice of a slightly lower continuum with respect to GCFT, has induced a migration from high  $b$  values and small column densities toward smaller Doppler widths.

**Fig. 4.** Doppler parameter distribution for the  $\text{Ly}\alpha$  lines in Tab. 2, out of 8 Mpc from the quasar PKS 2126–158.

The Doppler width distribution of the complete ( $\log N_{\text{HI}} \geq 13.3$ ) sample of  $\text{Ly}\alpha$  lines is shown in Fig. 4.

Using the standard assumption that line broadening is due exclusively to thermal motion, the relation between Doppler parameter and temperature,  $b^2 = 2kT/m$ , (where  $k$  is the Boltzmann constant and  $m$  is the hydrogen mass) implies that the peak value  $b \simeq 25 \text{ km s}^{-1}$  corresponds to a cloud temperature of  $T \sim 38000 \text{ K}$ .

The  $\text{Ly}\alpha$  sample contains 21 lines, i.e.  $\simeq 14.5 \%$ , with  $10 \leq b \leq 20 \text{ km s}^{-1}$ , and 12 lines, i.e.  $\simeq 8.3 \%$ , with  $15 \leq b \leq 20 \text{ km s}^{-1}$ . Such percentages are almost halved compared with those found in the previous work by GCFT. Nonetheless, it has to be noted that the peak value of the  $b$  distribution is roughly the same for the two samples.

The nature of the distribution of  $\text{Ly}\alpha$  clouds Doppler parameters has led in the past to controversies. Pettini et al. (1990) found  $\text{Ly}\alpha$  lines with a median Doppler parameter of  $17 \text{ km s}^{-1}$  and a strong intrinsic correlation between Doppler width and column density. From these results a scenario of very cool, dense and practically neutral clouds emerged, in contrast with previous models. Starting from data with similar resolution, Carswell et al. (1991) following different selection and analysis criteria obtained significantly larger average and median Doppler parameters and, above all, no  $b - N$  correlation. Our median  $b$  value is intermediate between the results of Pettini et al. and that



of Carswell et al. and it agrees with recent result at very high resolution (Hu et al. 1995; Lu et al. 1996).

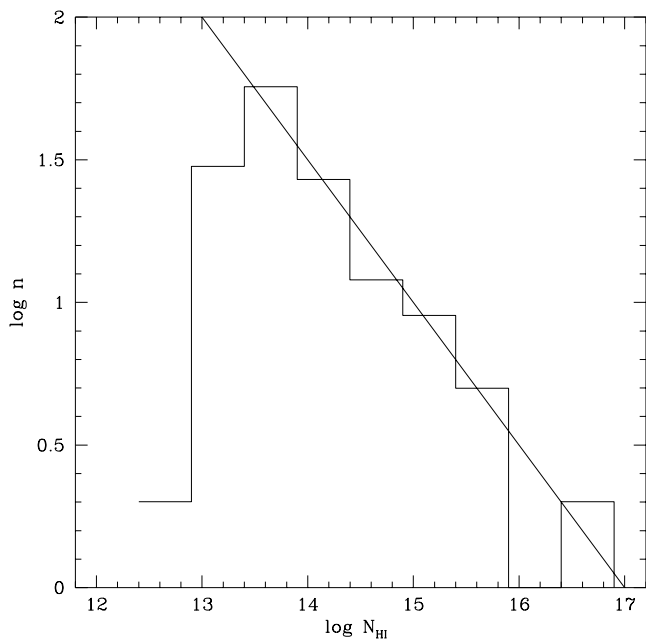


**Fig. 5.** Column density distribution of the Ly $\alpha$  lines out of 8 Mpc from the quasar PKS 2126–158. The overplotted solid line represents a power-law distribution,  $\propto N^{-\beta}$ , with  $\beta = 1.5$  (Hu et al. 1995; Giallongo et al. 1996).

The column density distribution of our Ly $\alpha$  line sample is shown in Fig. 5. As shown in Fig. 2, for values  $\log N_{\text{HI}} \lesssim 13.3$  a selection bias is expected: only lines with small Doppler parameters are detectable. This is confirmed by the drop of the column density distribution below this  $\log N_{\text{HI}}$  value. The shape of the distribution is in agreement with the power-law fit  $N^{-\beta}$ , with  $\beta \simeq 1.5$ , obtained in the recent works by Hu et al. (1995) and Giallongo et al. (1996).

The number density of lines per unit redshift, in the wavelength interval  $\lambda\lambda 4380 - 5065 \text{ \AA}$  for Ly $\alpha$  absorptions with  $\log N_{\text{HI}} \geq 14$ , is in good agreement with the cosmological redshift distribution (Giallongo et al. 1996).

## 5. Identification and analysis of the metal systems

As a first guess, heavy-element systems have been identified on the basis of the line list presented by GCFT. Eventually, other element lines have been added to the previously found systems, making use of a list of the lines most frequently observed in QSO absorption spectra, derived from Morton (1991). The oscillator strengths of Si II  $\lambda 1526$  and Si II  $\lambda 1304$  have been corrected according to Verner et al. (1996).

As for the Ly $\alpha$  lines, the operation of fitting has been carried out within the context FITLYMAN of the reduction package MIDAS. In the case of the complex profiles observed for the heavy-element lines, a minimum number of components needed to obtain a  $\chi^2 < 1$  and a good fit was deduced from the C IV profiles (or, in one case at low redshift, from the Mg II one).

Then an identification programme, based on the method of Young et al. (1979), has been applied to the newly observed lines that seemed not to belong to existing systems.

Besides the systems previously found at lower resolutions (Young et al. 1979; Sargent et al. 1988; GCFT), we show two systems identified on the basis of the C IV doublet, whose column densities and equivalent widths were too weak to be detected in previous observations. We do not confirm the existence of the system at  $z = 2.33$  found by GCFT, whose lines were all inside the Ly $\alpha$  forest. Six of the twelve systems show a multicomponent substructure, with a velocity extent up to  $\sim 350 \text{ km s}^{-1}$ . We have not adopted any velocity window, or other strict rules for the classification into systems versus sub-systems. We have simply considered as one system those groups of lines for which a simultaneous fit was required because of the superposition of the various line profiles.

### 5.1. Notes on individual systems

Each system has been assigned a letter, from A to L, in order of increasing redshift.

#### 5.1.1. The metal system at $z_{\text{abs}} = 0.6631 - A$

The two strongest Ca II doublets of this system have been already observed by GCFT. Furthermore, two other components have been fitted, together with the respective Mg II doublets. The two components with higher column density values show also Mg I  $\lambda 2852$ .

The total spread in velocity of the system is  $\sim 215 \text{ km s}^{-1}$ .

#### 5.1.2. The metal system at $z_{\text{abs}} = 2.3941 - B$

The existence of this system was formerly suggested by Young et al. and subsequently confirmed by Sargent et al. (1990) and by GCFT.

The C IV  $\lambda 1548$  line at  $z_{\text{abs}} = 2.3932$  is blended with the Si IV  $\lambda 1393$  of the complex system H, but the other line of the doublet has a very clean profile that guarantees the reliability of the fit.

We have found another component by means of the C IV doublet, which is slightly separated ( $\sim 100 \text{ km s}^{-1}$ ) from the others. The maximum separation among the three is  $\sim 180 \text{ km s}^{-1}$ .

Corresponding to two lower redshift components we have fitted the Si IV doublets and at  $z_{\text{abs}} = 2.3932$  also Si II  $\lambda 1526$ , Si II  $\lambda 1808$  and Al II  $\lambda 1670$ .

### 5.1.3. The metal system at $z_{\text{abs}} = 2.4597 - \text{C}$

This system, identified by Sargent and collaborators (1988), shows two C IV doublets. Relative to the stronger component, we observe an uncertain Fe II  $\lambda 1260$  and the Ly $\alpha$ , both in a region with low  $s/n$  ratio. The Si IV doublets, if present, are blended with the stronger C II complex of system E.

### 5.1.4. The metal system at $z_{\text{abs}} = 2.5537 - \text{D}$

We have identified this low column density C IV doublet in a region with high  $s/n$  ratio and absence of lines. This new system does not show any other metallic line associated with it.

### 5.1.5. The metal system at $z_{\text{abs}} = 2.6378 - \text{E}$

This multicomponent system shows ten sub-features, three more than in GCFT, with a total spread in velocity of  $\sim 286 \text{ km s}^{-1}$ . The number of components and the relative redshifts have been derived from the observation of the C IV lines which lie outside the Ly $\alpha$  forest.

Lines shortward of the Ly $\alpha$  emission are difficult to examine because they are blended with H I lines. In these cases (e.g. C II  $\lambda 1335$ ) we have identified and fitted any components in coincidence with C IV components. Nevertheless, the  $b$  and  $N$  values of these lines, and even their existence, are to be considered doubtful.

In addition to the elements found by GCFT, we have fitted Si III  $\lambda 1206$ , Si II  $\lambda 1304$  and  $\lambda\lambda 1190, 1193$ , all in a region of the spectrum with low  $s/n$  ratio.

The corresponding Ly $\alpha$  line has been fitted separately. As a matter of fact, it was so strongly saturated that even the observation of the Ly $\beta$  did not help in the determination of its profile.

### 5.1.6. The metal system at $z_{\text{abs}} = 2.6788 - \text{F}$

A clear C IV doublet, first identified by Sargent et al. (1988), is observed outside the Ly $\alpha$  forest; all the other lines of this system lie inside it. At the same redshift of C IV, Si IV doublet and N V doublet have been found.

Si IV doublet has been fitted using Si IV  $\lambda 1402$  only, since Si IV  $\lambda 1393$  is blended with a wide Ly $\alpha$  line. Besides, it shows a possible second component separated by  $\sim 20 \text{ km s}^{-1}$  from that identified by the C IV. A Si II  $\lambda 1260$  is observed at this last redshift, while the existence of the other lines found by GCFT is not confirmed.

### 5.1.7. The metal system at $z_{\text{abs}} = 2.7281 - \text{G}$

This system has been identified by the C IV doublet, which presents two components separated by  $\sim 30 \text{ km s}^{-1}$ .

Unlike in GCFT, Ly $\alpha$  and Si IV doublet, even if extremely weak, have been fitted. Other lines, whose identification is uncertain, are: Si III  $\lambda 1206$  blended with the

multicomponent Si II of system H and Fe II  $\lambda 1260$  blended with a Ly $\alpha$  line.

### 5.1.8. The metal system at $z_{\text{abs}} = 2.7689 - \text{H}$

This is the most complex system found in our spectrum. It appears as a blended feature of  $\Delta v \simeq 350 \text{ km s}^{-1}$ .

We observe seven C IV doublets and four possible very weak lines of C IV  $\lambda 1548$ . Four more components have been identified using low-ionization lines falling outside the Ly $\alpha$  forest, and all the lines unambiguously identified in the Ly $\alpha$  forest have been fitted.

Besides the lines fitted by GCFT, we have added those of Si II  $\lambda 1304, \lambda 1260, \lambda 1190, \lambda 1193$  and the fine-structure excited level C II  $\lambda 1335$ . No fine-structure line of Si II has been observed.

As for the other complex system, E, the Ly $\alpha$  line has been observed but not fitted together with the other elements. The presence of the corresponding Ly $\beta$  line does not help much because of the strong saturation.

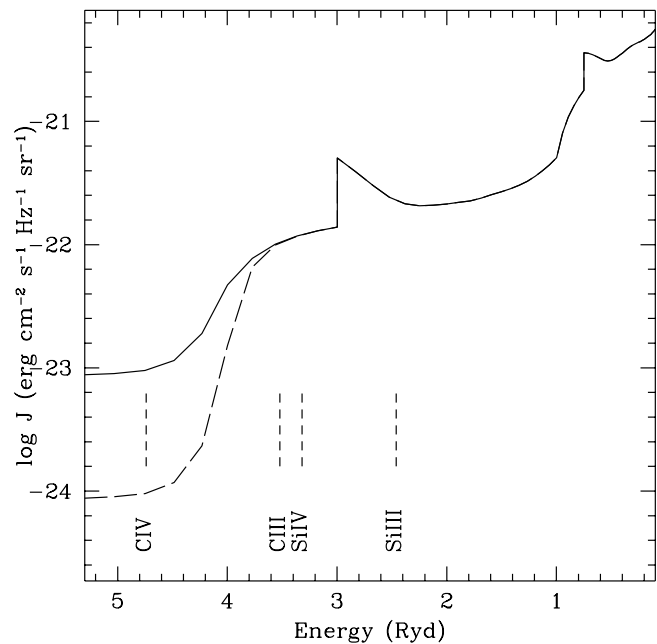


**Fig. 6.** The shape of the ultraviolet background at the epoch  $z=2.9$ . Continuous line: as computed by Haardt and Madau (1997); dashed line: with an increased (of a factor 10) jump around 4 Ryd. The ionization potentials of a few ions are shown.

### 5.1.9. The metal system at $z_{\text{abs}} = 2.8195 - \text{I}$

Meyer and York (1987) identified this system as a single C IV doublet. We have added the identifications of O

I  $\lambda 1302$ , Si III  $\lambda 1206$ ,  $\text{Ly}\alpha$ ,  $\text{Ly}\beta$  and  $\text{Ly}\gamma$ , while the existence of Si II  $\lambda 1304$ ,  $\lambda 1309$  is uncertain due to severe blending.

None of the low-ionization lines reported by GCFT have been observed, apart from Al II  $\lambda 1670$  that has become a C IV at  $z = 3.216542$ .

#### 5.1.10. The metal system at $z_{\text{abs}} = 2.9072 - \text{J}$

This C IV system (Meyer & York 1987) shows also Si III  $\lambda 1206$ , Si IV  $\lambda\lambda 1393, 1402$ ,  $\text{Ly}\alpha$   $\text{Ly}\gamma$  and  $\text{Ly}\delta$ .

#### 5.1.11. The Lyman limit system at $z_{\text{abs}} = 2.9675 - \text{K}$

This is a Lyman-limit system identified by Sargent et al. (1990).

The  $\text{Ly}\alpha$  line of this system probably has a complex structure which has not been possible to disentangle even examining the corresponding  $\text{Ly}\gamma$ , still badly saturated.

At high resolution, the C IV identification is doubtful (a wavelength discrepancy of about  $0.5 \text{ \AA}$  is observed between the two components of the doublet). We have identified and fitted a very weak Si IV  $\lambda 1393$  and Si III (possibly contaminated by  $\text{Ly}\alpha$ ). The existence of the N V doublet is not verifiable since a wide H I line is present at that wavelength.

#### 5.1.12. The metal system at $z_{\text{abs}} = 3.216542 - \text{L}$

This possible system, previously unknown, shows a C IV doublet (the C IV  $\lambda 1548$  line was identified as Al II  $\lambda 1670$  at  $z = 2.81959$  by GCFT) and a Si IV doublet outside the Lyman forest. We have fitted also the  $\text{Ly}\alpha$  line and Si III  $\lambda 1206$  in the forest.

For the systems I and J the reliability of the fit of the Lyman series allows a measure of the metallicity. In system K it is possible to put an upper limit to it on the assumption of  $\log N_{\text{HI}} \geq 17$ . We have used the standard photoionization code CLOUDY (Ferland 1996), following the same approach described in detail in Savaglio et al. (1997).

In the analysis of system J, if the standard UV background at  $z=2.9$  (Haardt and Madau 1996) is adopted and the size of the cloud is assumed not smaller than 20 Kpc, we end up with an unplausibly high overdensity of silicon with respect to carbon,  $\gtrsim 50$ . To obtain a more realistic  $[\text{Si}/\text{C}] \lesssim 1$  the cloud size should decrease substantially below 10 kpc. Incongruities of this type are not uncommon, as reported by Songaila and Cowie (1996) and Savaglio et al. (1997). Several processes may increase the SiIV/CIV ratio: a photoionizing background dominated by local sources, non-equilibrium temperatures and non-uniform radiation fields (Giroux and Shull 1997). In Savaglio et al. (1997) and here we have explored the possibility of an enhanced break at 4 Ryd in the metagalactic background radiation, as could be originated by a contribution of primeval galaxies in addition to the standard

QSO background. With a jump increased of a factor 10 at 4 Ryd (Fig. 6), the observed line ratios turn out to be compatible, assuming a cloud size of 30 kpc, with a metallicity  $-2.5$  dex solar and an overabundance of silicon with respect to carbon of a factor 5-6.

The analysis of systems I and K, under the assumption of the same UV background with an enhanced jump at 4 Ryd and cloud sizes  $\gtrsim 15$  kpc, provides metallicities of  $\simeq -2.2$  and  $\lesssim -2.7$ , respectively. System I, again, requires an overabundance of silicon with respect to carbon of a factor 4 that would become much larger if the standard UV background is assumed.

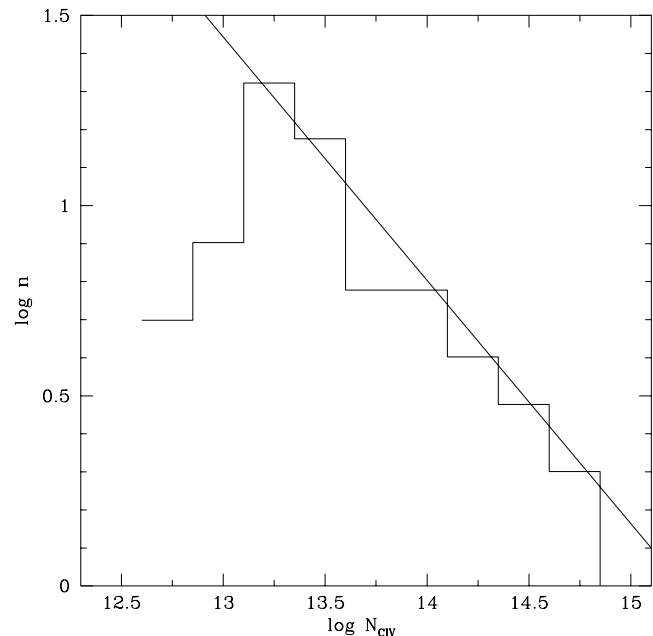


**Fig. 7.** Histogram of the logarithmic number of C IV absorptions as a function of the column density. The solid line represents a power-law:  $N_{\text{CIV}}^{-\beta}$ ,  $\beta = 1.64$  (Petitjean & Bergeron 1994).

## 6. Statistics of C IV systems

In order to investigate the statistical properties of C IV systems, an enlarged sample has been created by merging the present data with those recently obtained at similar resolution for Q0000–26 (Savaglio et al. 1997) and Q0055–269 (Cristiani et al. 1995). All the spectra have been analyzed in a homogeneous way according to the same procedures described in sections 2 and 3.

### 6.1. Doppler parameter and column density

The distribution of C IV column densities is shown in Fig. 7. It can be described as a single power-law distri-

bution,  $dn/dN \propto N^{-\beta}$ , with  $\beta = 1.64$  (in agreement with Petitjean & Bergeron 1994), down to a completeness limit  $\log N_{\text{CIV}} \sim 13.3$ .

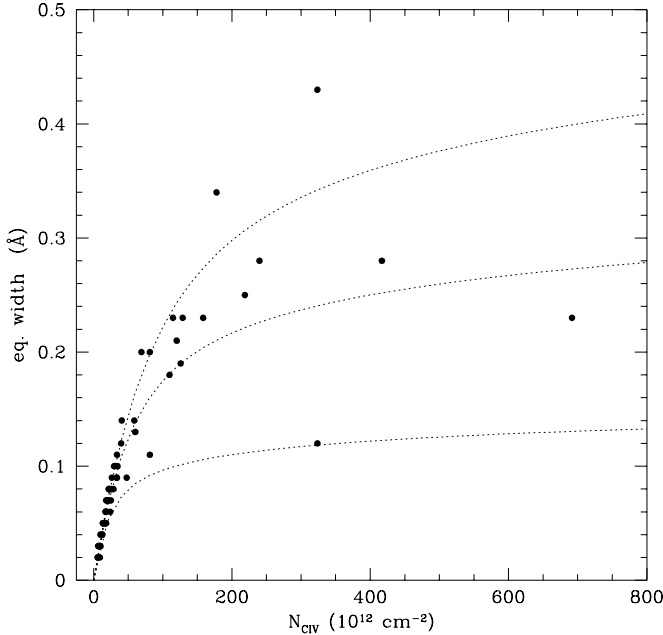


**Fig. 8.** Rest equivalent width of single C IV system components as a function of the column density (in units of  $10^{12} \text{ cm}^{-2}$ ). The overplotted curves of growth have been computed for values  $b = 6, 14, 22 \text{ km s}^{-1}$  of the Doppler parameter (Spitzer 1978; Press & Rybicki 1993).

The distribution of the Doppler parameters for the same C IV lines has a mode of  $\simeq 14 \text{ km s}^{-1}$  and a standard deviation  $\sigma_b \simeq 8 \text{ km s}^{-1}$ . A simple derivation of the expected  $\langle b_{\text{CIV}} \rangle$  from the corresponding  $\langle b_{\text{Ly}\alpha} \rangle$ , with the hypothesis of pure thermal broadening with a single temperature would provide  $\langle b_{\text{CIV}} \rangle \simeq 7 \text{ km s}^{-1}$ . This indicates either that turbulent motions are present or some of the lines are blends of subcomponents, which would be separated only by observations with higher spectral resolution and  $s/n$ .

Figure 8 shows the equivalent widths, estimated from the  $b$  and  $N_{\text{CIV}}$  values derived for each subcomponent by profile fitting, versus the column density. It can be seen that most of the lines are on the linear part of the curve of growth, at least for  $N_{\text{CIV}} < 10^{14} \text{ cm}^{-2}$ . Curves of growth have been drawn for values of the Doppler parameter  $b_{\text{CIV}} = 6, 14, 22 \text{ km s}^{-1}$ .

## 7. Clustering of C IV clouds

### 7.1. Statistical tools

We have adopted as a statistical tool the two-point correlation function (TPCF), defined as the excess, due to clustering, of the probability  $dP$  of finding a cloud in a volume  $dV$  at a distance  $r$  from another cloud:

$$dP = \Phi(z) [1 + \xi(r)] dV \quad (1)$$

where  $\Phi(z)$  is the average space density of the clouds as a function of  $z$ . The TPCF is known to be a satisfactory estimator when used to investigate weak clustering on scales considerably smaller than the total interval covered by the data. The binning, intrinsic to this method, causes a loss of information, but the ease in visualizing its results and in including observational effects in the computing codes have made of the TPCF one of the favorite statistical estimators in cosmology.

In practice the observations provide the redshifts of the absorption lines that, due to peculiar motions, are not immediately transformed in comoving distances. Therefore the TPCF is generally computed in the velocity space, making use of the formula (Peebles 1980)

$$\xi(v, \Delta v) = \frac{n_{\text{obs}}(v, \Delta v)}{n_{\text{exp}}(v, \Delta v)} - 1 \quad (2)$$

where  $n_{\text{obs}}$  is the number of observed line pairs with velocity separations between  $v$  and  $v + \Delta v$  and  $n_{\text{exp}}$  is the number of pairs expected in the same interval from a random distribution in redshift.

At the small velocity separation we are dealing with, the variation of the distance scale with cosmic time can be neglected and the velocity difference can be simply deduced from the redshift difference (Sargent et al. 1980)

$$\Delta v = \frac{c(z_2 - z_1)}{1 + (z_1 + z_2)/2} \quad (3)$$

where  $\Delta v$  is the velocity of one cloud as measured by an observer in the rest frame of the other.

In our line sample  $n_{\text{exp}}$  is obtained by averaging 5000 numerical simulations of the observed number of redshifts, trying to account for all the relevant cosmological and observational effects. In particular the set of redshifts is randomly generated in the same redshift interval as the data according to the cosmological distribution  $\propto (1 + z)^\gamma$ , where  $\gamma$  has been taken equal to  $-1.2$  (Sargent et al. 1988). Observed pairs with a velocity splitting  $\Delta v < 30 \text{ km s}^{-1}$  have been merged, while simulated ones have been excluded in the estimate of  $n_{\text{exp}}$ , because of the intrinsic line blending due to the typical widths of the C IV lines.

The TPCF for the C IV clouds is presented in Fig. 9 with  $60 \text{ km s}^{-1}$  bins. A strong clustering signal is detected at small velocity separations ( $\Delta v < 1000 \text{ km s}^{-1}$ ). At larger scales no significant signal is found, in particular the peaks observed in the TPCF at  $\sim 3360 \text{ km s}^{-1}$ ,  $\sim 7140 \text{ km s}^{-1}$  and at  $\sim 9840 \text{ km s}^{-1}$  are aliases corresponding to

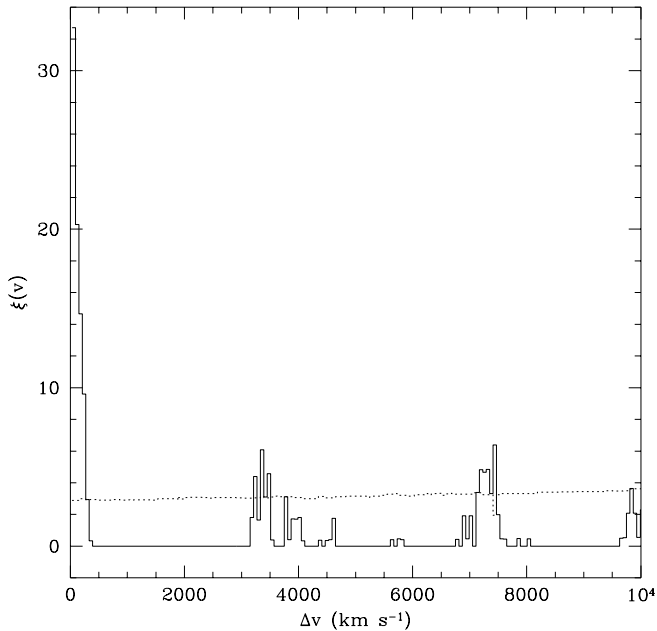


**Fig. 9.** Two point correlation function at large velocity separations for the C IV systems. The dotted line shows the 95 % confidence level.

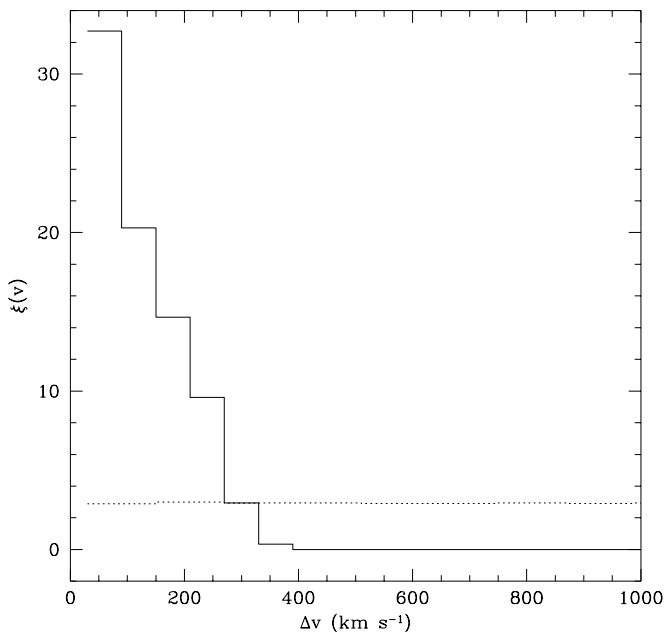


**Fig. 10.** Two point correlation function at small velocity separations for the C IV systems. The dotted line shows the 95 % confidence level

the coupling of the low  $\Delta v$  (high frequency) power with the window function.

The present data have adequate resolution to allow a further investigation of the distribution on scales smaller than  $1000 \text{ km s}^{-1}$ . The TPCF for velocity separations in the range  $30 \leq \Delta v \leq 1000$  is shown in Fig. 10. In this velocity interval 48 pairs are observed, while  $\sim 10$  are predicted for a homogeneous distribution.

Similar results, with a significant correlation on scales up to  $200\text{--}300 \text{ km s}^{-1}$ , have been obtained in the works by Petitjean and Bergeron (1994), Womble et al. (1996) and Songaila and Cowie (1996), carried out at comparable resolution.

The velocity scale at which the maximum clustering signal is observed is comparable with the extension of the complex metal absorption features in the spectrum. This suggests, as already noticed by Petitjean and Bergeron (1994), that we are not seeing clustering of “galaxies” but of gas clouds within the same galactic halo.

Other authors (Sargent et al. 1988; Heisler et al. 1989) report, on the basis of large samples of QSOs observed at relatively low resolution (a few Angstrom), significant correlation of C IV lines up to scales of  $600\text{--}1000 \text{ km s}^{-1}$ . If the resolution of the present data is degraded to the level typical of those investigations (e.g. a resolution of  $77 \text{ km s}^{-1}$ ), a compatible result is obtained, with  $\xi(0 < \Delta v < 1000 \text{ km s}^{-1}) \simeq 2.0 \pm 0.9$ .

The correlation on scales larger than  $1000 \text{ km s}^{-1}$  reported by Heisler et al. (1989) is not reproduced. It has to be noted, however, that it appears to be the result of the inclusion in their sample of one “exceptional” object, 0237-233.

## 7.2. Correlations with the column density

It has long been assessed that a correlation exists between the equivalent width of metal absorption systems and their number of components (Wolfe 1986; Petitjean & Bergeron 1990; Petitjean & Bergeron 1994).

In Fig. 11 the total equivalent width is plotted versus the number of components for the C IV absorption systems. The dashed line represents the best linear fit for all the points.

The number of components, however, is highly dependent on the spectral resolution and on subjective taste. To overcome this problem, we examined the maximum velocity separation in a given system versus the total equivalent width (Fig. 12). A correlation is apparent and the dashed line is, again, the best linear fit.

The observed trends suggest that the clustering amplitude of the C IV lines could be a function of the column density.

In order to further investigate this issue, in Fig. 13 the amplitude of the TPCF (in the bin  $30 < \Delta v < 90 \text{ km s}^{-1}$ ) is plotted as a function of the median value of the C IV column density. The upper right point represents the result

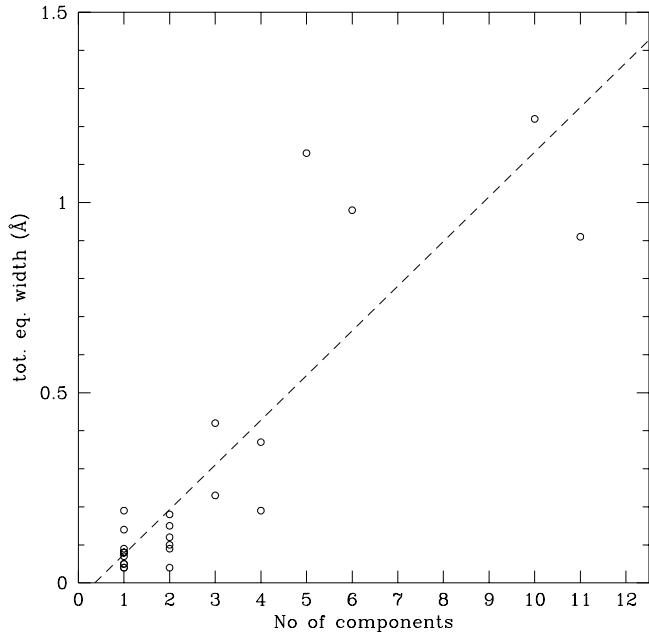


**Fig. 11.** Total equivalent width of C IV systems versus the corresponding number of components. The dashed line is the linear correlation best fit for all points.

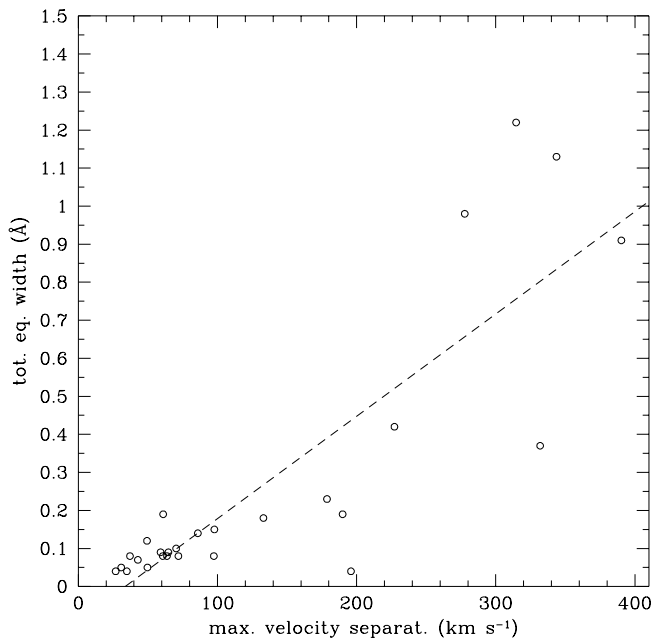


**Fig. 12.** Total equivalent width of C IV systems versus the corresponding maximum velocity separation. The dashed line is the linear correlation best fit.

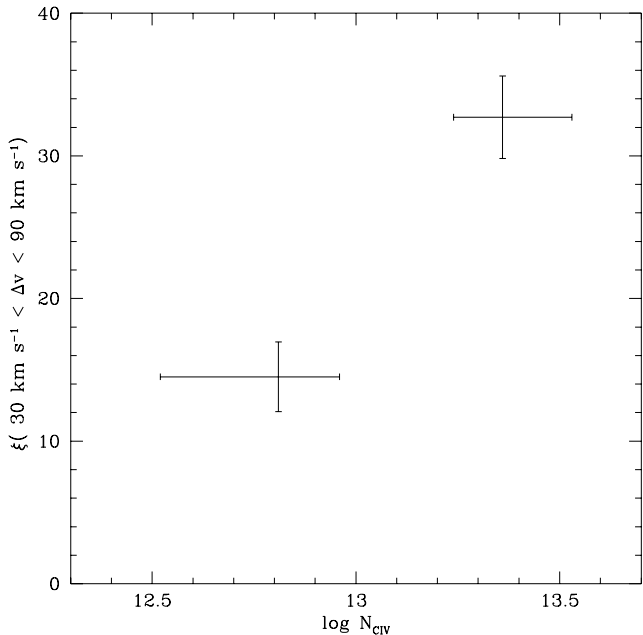


**Fig. 13.** Amplitude of the clustering of C IV lines as a function of the column density. The upper right point has been obtained for the present enlarged sample of C IV lines. The lower left point has been derived from the data of the QSO 1422+231 (Songaila & Cowie 1996). The vertical bars represent  $1\sigma$  poissonian uncertainties in the determination of the TPCF while the horizontal ones show the 68% confidence interval of the column densities.

obtained in this work for the C IV absorptions in the enlarged sample. The lower left point comes from the lower column density sample obtained by Songaila and Cowie (1996) for the QSO 1422+231. The TPCF has been computed, also for the latter data, according to the procedure described in § 7.1. Lines of lower column density show indeed a smaller amplitude of the TPCF at  $30 < \Delta v < 90$  km s $^{-1}$ .

The correlation of the clustering amplitude with column density is analogous to what has been observed for Ly $\alpha$  lines (Cristiani et al. 1997) and it is qualitatively consistent with a picture of gravitationally induced correlations.

## 8. Conclusions

We have presented high-resolution spectra of the quasar PKS 2126–158.

The analysis of the Ly $\alpha$  forest shows that:

1. The peak value of the Doppler parameter distribution is  $\sim 25$  km s $^{-1}$ . This value is large enough to be in agreement with a standard ionization model, but not too high ( $b \gtrsim 30$ ) to make the Ly $\alpha$  clouds contribution

to baryonic matter exceed the standard nucleosynthesis value (Hu et al. 1995).

2. The plot of the statistical sample of Ly $\alpha$  lines in the  $b$ –log  $N$  plane shows no significant correlation between the two parameters.
3. The column density distribution shows a cutoff, due to incompleteness and blending, for  $\log N_{\text{HI}} \lesssim 13.3$ , for higher values it is well described by a power-law  $dn/dN_{\text{HI}} \propto N_{\text{HI}}^{-\beta}$  with  $\beta = 1.5$  (Hu et al. 1995; Giallongo et al. 1996).
4. The number density of lines per unit redshift is in agreement with a standard power-law evolution of the type  $dn/dz \propto (1+z)^\gamma$  with  $\gamma = 2.7$  (Giallongo et al. 1996).

Clustering properties of the Ly $\alpha$  lines have been investigated in another paper (Cristiani et al. 1997). Ly $\alpha$  of higher column density ( $\log N_{\text{HI}} \gtrsim 13.8$ ) are found to cluster significantly on scales around  $100 \text{ km s}^{-1}$ .

From the analysis of metal absorptions the following results have been obtained:

1. Two new C IV absorption systems have been detected at  $z = 3.2165$  and  $z = 2.5537$ .
2. A mean metallicity of  $\sim -2.5$  dex solar has been found using the metal systems at  $z = 2.8195$ ,  $z = 2.9072$  and  $z = 2.9675$ . In order to make the column densities of the intervening systems compatible with realistic assumptions about the cloud sizes and the [Si/C] ratios, it is necessary to assume an increase of a factor 10 in the jump at 4 Ryd of the standard spectrum of the ionizing UV background (Haardt & Madau 1997).
3. Merging the present data with those obtained at comparable resolution for the two quasars Q0055-26 and Q0000-26, has provided a relative large sample (71 doublets) of C IV absorptions, complete down to a column density  $\log N_{\text{CIV}} \simeq 13.3$ . The C IV column density distribution is well fitted by a single power-law, with  $\beta = 1.64$ .
4. The mode of the Doppler parameter distribution is  $b_{\text{CIV}} \simeq 14 \text{ km}^{-1}$ .
5. The clustering properties of the individual components of the C IV features have been investigated making use of a TPCF in the velocity space. A significant signal is obtained for scales smaller than  $200 - 300 \text{ km s}^{-1}$ ,  $\xi(30 < \Delta v < 90 \text{ km s}^{-1}) = 32.71 \pm 2.89$ . The result is consistent with previous findings (Sargent et al. 1988; Heisler et al. 1989) when the increased resolution and  $s/n$  ratio of the present data is taken into account.
6. Correlations between total equivalent widths and number of components and between total equivalent widths and velocity spread of the individual C IV systems are observed. The two-point correlation functions for lower column density C IV absorption systems, recently estimated by Womble et al. (1997) and Songaila and Cowie (1996), show a weaker signal than the present data.

These three pieces of evidence suggest a trend of decreasing clustering amplitude with decreasing column density. An analogous behaviour has been observed for Ly $\alpha$  lines by Cristiani et al. (1997).

*Acknowledgements.* We thank P. Madau, C. Porciani and S. Savaglio for enlightening discussions. B SC acknowledges the support of the ASI contract 95-RS-38 and of the TMR-network of the European Community “Galaxy Formation and Evolution”.

## References

- Bajtlik S., Duncan R.C., Ostriker J.P., 1988, ApJ 327, 570  
 Bechtold J., Green R.F., York D.G., 1987, ApJ 312, 50  
 Carswell R.F., Whelan J.A.J., Smith M.G., Boksenberg A. and Tytler D. 1982, MNRAS 198, 91  
 Carswell R.F., Lanzetta K.M., Parnell H.C., Webb J.K., 1991, ApJ 371, 36  
 Chernomordik V.V., 1995, ApJ 440, 431  
 Cowie L.L., Songaila A., Kim T., Hu E.M., 1995, AJ 109, 1522  
 Cristiani S., D’Odorico S., Fontana A., Giallongo E., Savaglio S., 1995, MNRAS 273, 1016  
 Cristiani S., D’Odorico S., D’Odorico V., et al., 1997, MNRAS 285, 209  
 D’Odorico S., 1990, ESO The Messenger 61, 51  
 Ferland G.J., 1996, Hazy, a Brief Introduction to Cloudy, University of Kentucky Department of Physics and Astronomy Internal Report  
 Fernández-Soto A., Lanzetta K.M., Barcons X., et al., 1996 ApJ 460, L85  
 Fontana A., Ballester P., 1995, ESO The Messenger 80, 37  
 Giallongo E., Cristiani S., Fontana A., Trevese D., 1993, ApJ 416, 137  
 Giallongo E., Cristiani S., D’Odorico S., Fontana A., Savaglio S., 1996, ApJ 466, 46  
 Giroux M.L., Shull J. M., 1997 preprint astro-ph/9701160  
 Haardt F., Madau P., 1996, ApJ 461, 20  
 Heisler J., Hogan C., White S.D.M. 1989, ApJ 347, 52  
 Hu E.M., Kim T., Cowie L.L., Songaila A., Rauch M. 1995, AJ 110, 1526  
 Jauncey D.L., Wright A.E., Peterson B.A., Condon J.J., 1978, ApJ 223, L1  
 Lanzetta K.M., Bowen D.V., Tytler D., Webb J.K., 1995, ApJ 442, 538  
 Lu L., Wolfe A.M., Turnshek D.A., 1991, ApJ 367, 19  
 Lu L., Sargent W.L.W., Womble D.S., Takada-Hidai M. 1996, ApJ 472, L509  
 Lynds C.R., 1971, ApJ 174, L73  
 Meiksin A., Bouchet R.F., 1995, ApJ 448, L85  
 Meyer D.M., York D.G., 1987, ApJ 315, L5  
 Morton D.C., 1991, ApJS 77, 119  
 Peebles P.J.E., 1980, The Large Scale Structure of the Universe. Princeton Univ. Press, Princeton  
 Petitjean P., Bergeron J., 1990, A&A 231, 309  
 Petitjean P., Bergeron J., 1994, A&A 283, 759  
 Pettini M., Hunstead R.W., Smith L.J., Mar D.P., 1990, MNRAS 246, 545  
 Press W.H., Rybicki G.B., 1993, ApJ 418, 585  
 Rauch M., Carswell R.F., Webb J.K., Weymann R.J., 1993, MNRAS 260, 589

- Sargent W.L.W., Young P.J., Boksenberg A., Tytler D., 1980, ApJS 42, 41
- Sargent W.L.W., Young P.J., Schneider D.P., 1982, ApJ 256, 374
- Sargent W.L.W., Boksenberg A., 1983. In: 24th Liège Astrophysical Colloquium. 518, Quasar and Gravitational Lenses
- Sargent W.L.W., Boksenberg A., Steidel C.C., 1988, ApJS 68, 539
- Sargent W.L.W., Steidel C.C., Boksenberg A., 1989, ApJS 69, 703
- Sargent W.L.W., Steidel C.C., Boksenberg A., 1990, ApJ 351, 364
- Savaglio S., Cristiani S., D'Odorico S., et al., 1997, A&A 318, 347
- Songaila A., Cowie L.L., 1996, AJ 112, 335
- Spitzer L. Jr, 1978, Physical Processes in the Interstellar Medium. John Wiley and Sons, New York, 52
- Stone R.P.S., Baldwin J.A., 1983, MNRAS 204, 347
- Tytler D., Fan X-M., Burles S., et al., 1995, in: Meylan G. (ed.) QSO Absorption Lines, ESO Astrophysics Symposia, Springer: Heidelberg, 289
- Verner D.A., Verner E.M., Ferland G.J., 1996, BAAS 188, 5418
- Webb J.K., Barcons X., 1991, MNRAS 250, 270
- Wolfe A., 1986, in: Bregman J., Lockman J. (eds.) Proc. NRAO Conf. on Gaseous Halos of Galaxies. NRAO SP, 259
- Womble W.S., Sargent W.L.W., Lyons R.S., 1996, in: Bremer M.N., (eds.) Proc. of the Kluwer Conf. on Cold Gas at High Redshift
- Young P.J., Sargent W.L.W., Boksenberg A., Carswell R.F., Whelan J.A.J., 1979, ApJ 229, 891
- Young P.J., Sargent W.L.W., Boksenberg A., 1982, ApJS 48, 455

A